PCCP

Pressure and temperature dependence of the gas-phase reaction of silylene with dimethyl ether

Ula N. Alexander,[a] Keith D. King*[b] and Warren D. Lawrance[a]

[a] *School of Chemistry, Physics and Earth Sciences, Flinders University, GPO Box 2100, Adelaide SA 5001, Australia*
[b] *Department of Chemical Engineering, Adelaide University, SA 5005, Australia. E-mail: kking@chemeng.adelaide.edu.au*

Received 2nd January 2001, Accepted 25th May 2001
First published as an Advance Article on the web 29th June 2001

Gas-phase reaction rate constants for the reaction of silylene, SiH_2, with dimethyl ether, CH_3OCH_3 have been determined over the temperature range 294–441 K and at total pressures of inert bath gas (Ar or SF_6) over the range 30–850 Torr. The second-order rate constants are pressure dependent, even up to the maximum pressure investigated of 850 Torr, and the rate constants decrease with increasing temperature, indicating that the reaction proceeds *via* the formation of a complex. At the highest temperature studied (441 K), the experimental decay curves do not return to the baseline. This is attributed to the system reaching equilibrium, with SiH_2 being produced by dissociation of the complex, and provides direct experimental evidence for the formation of the complex. Analysis of the decay curves provided an experimental determination of the equilibrium constant, K_{eq}, at 441 K. The high-pressure rate constants, obtained by extrapolation of the experimental data using RRKM/master equation modelling, yield the Arrhenius parameters $\log(A/\mathrm{cm^3\ molecule^{-1}\ s^{-1}}) = -7.6 \pm 0.4$ and $E_a = 9.3 \pm 2.8$ kJ mol^{-1}. The RRKM/master equation modelling gives a well depth for the SiH_2–CH_3OCH_3 complex of 87 kJ mol^{-1}. This compares with a value of 88.4 ± 1.7 kJ mol^{-1} determined from K_{eq} at 441 K. *Ab initio* calculations, performed at the MP2/6-311+G** level of theory, give a well-depth for the complex of 82.9 kJ mol^{-1}, in excellent agreement with this value.

1. Introduction

Silylene, SiH_2, is a reactive intermediate important to a number of industrial processes. For example, it is formed when silanes are pyrolysed during the chemical vapour deposition (CVD) process used to deposit thin silicon films onto substrates during the manufacture of semi-conductor components. The desire to determine the reactions and kinetic behaviour of this key reactive intermediate within the silicon CVD process has been a major force driving the interest in the study of SiH_2 kinetics.[1] Besides the industrial relevance of SiH_2 kinetic studies, there is a desire to understand the fundamental chemistry of the simplest silylene and how its reactions compare to its Group 4 analogues, CH_2 and GeH_2.

Prior to 1985, silylenes were exclusively studied *via* indirect methods such as end-product analyses and relative rates.[2–4] These indirect studies are useful since they give a broad picture of the reactivity of silylenes and provide grounding for direct gas-phase experiments. Since 1985, direct time-resolved techniques in the gas phase have allowed more detailed study of the reaction kinetics,[5] including direct insight into reaction intermediates. In addition to the direct study of SiH_2 kinetics, reactions of dimethylsilylene, $SiMe_2$, have also been studied in some detail.[6–8]

The gas-phase reactions between SiH_2 and selected small inorganic molecules, alkanes, alkenes, alkynes and silanes have been investigated with varying levels of detail. Reviews such as those of Jasinski *et al.*[9] and Becerra *et al.*[10] provide a summary of the SiH_2 reactions that have been studied. The general picture that emerges is that SiH_2 reacts by insertion into certain types of sigma bonds and by addition across double and triple bonds. Insertion into C–H bonds (alkanes), H–H bonds (hydrogen) and Si–C bonds (substituted silanes) is much slower than insertion into Si–H bonds (silanes) and addition across multiple bonds (alkenes and alkynes). Examples of reactions showing a dependence of the reaction rate on total pressure include SiH_2 reaction with C_2H_4[11] and C_2H_2,[12] which are still pressure-dependent at 100 Torr, the highest pressure accessed experimentally. N_2O and Me_3SiH[10] are notable exceptions to the dependence of the reaction rate on total pressure.

The reactions of SiH_2 with organic analogues of water (*e.g.*, methanol, MeOH and dimethyl ether, Me_2O) are of importance to the study of silicone chemistry. They also represent an important class of reactions, namely SiH_2 with n-donor bases. However, to date they have received little attention.[10] Preliminary kinetics studies within our group of the reactions of SiH_2 with D_2O and CD_3OD have led to some unpublished data for these reactions at room temperature[13] and, in conjunction with Walsh's group, we have reported the results of a limited study of the reaction of SiH_2 with Me_2O.[14] We have now studied the reaction of SiH_2 with H_2O, MeOH and Me_2O, and some deuterated analogues, D_2O and CD_3OD, in detail, with the aim of determining the pressure and temperature dependence of the second-order rate constants for these reactions. The chosen reactants represent a series systematically substituted about the oxygen atom. We report here on a detailed study of the temperature and pressure dependence of SiH_2 reaction with Me_2O; papers discussing the other systems will follow.

The reaction of SiH_2 with Me_2O is expected to occur *via* the formation of a complex with significant charge transfer character.[15,16] The study by Becerra *et al.*[14] confirmed this. In the present work, RRKM/master equation modelling of the

experimental data and *ab initio* calculations are used to determine the well depth of the complex. In addition, we provide experimental evidence for the formation of the complex through the observation of equilibrium between the reactants and complex at elevated temperatures.

2. Experimental details

Experiments investigating reactions between SiH_2 and Me_2O were undertaken over the temperature range 294–441 K. The experimental system is based on that used in our extensive studies of CH_2 ($\tilde{a}\,^1A_1$) kinetics[17–22] and GeH_2 kinetics.[23,24] The temperature-variable reaction cell is described in ref. 20. We here give details pertinent to the SiH_2 experiments.

$SiH_2(0,0,0)$ was generated by 193 nm (ArF) excimer laser photolysis of phenylsilane, $PhSiH_3$, and probed by a single frequency cw laser tuned to 17 259.50 cm^{-1} (vac) which coincides with the rovibronic transition $^1B_1(0,2,0) \leftarrow {}^1A_1(0,0,0)$ 5_{05}.[25] 193 nm photolysis of $PhSiH_3$ produces SiH_2 in both the (0,0,0) and (0,1,0) vibrational states.[26] Chu *et al.* have shown that at total pressures above a few Torr collision-induced relaxation of vibrationally excited silylene is rapid[27] and, since our experiments are conducted at pressures >30 Torr, vibrational relaxation of the (0,1,0) SiH_2 to (0,0,0) is not expected to confound our measurements. This was confirmed by testing that the rate constants obtained using 248 nm photolysis, where much less (0,1,0) SiH_2 is produced, were the same as those obtained with 193 nm photolysis. Me_2O does not absorb at the photolysis wavelengths of 193 and 248 nm.

The probe laser is split into reference and signal beams. The signal beam is double passed through the reaction cell, giving a total absorption path length of 2 m, and then focussed onto one channel of a differential amplifier. The reference beam is imaged onto the second channel, with the laser noise thereby being subtracted from the resultant output. The output of the differential amplifier is averaged (64–256 photolysis laser shots) on a digital oscilloscope (Hewlett Packard 54510A) and the averaged trace transferred to a computer for analysis. To minimise non-silylene contributions to the signal, two sets of decay traces are recorded; one with the laser tuned to a SiH_2 absorption (signal) and one with the laser detuned from SiH_2 (background). The background is subtracted from the signal to provide the SiH_2 decay signal. The experiment is performed under conditions such that the reactions are pseudo-first order and the silylene signal decays exponentially. With the exception of the highest temperature data, decay traces were fitted to a bi-exponential function to account for both the rise and the decay features. At the highest temperature of 441 K traces did not return to the baseline. These traces were fitted with a tri-exponential function having a rise and two decay times. A minimum of three averaged traces were recorded and analysed at each reactant pressure. The signal levels were found to decrease with increasing total pressure.

The rate constants reported here were obtained with total cell pressures of 30–850 Torr. The $PhSiH_3$ pressure was typically 10–30 mTorr and the Me_2O pressure was typically varied in the range 0.5–3.5 Torr. Ar and SF_6 were used as the buffer gases with total pressures in the range 30–850 Torr (Ar) and 30–150 Torr (SF_6). The gases are flowed continuously through the sample cell to prevent the build up of reaction products. Gas flow rates are controlled using mass flow controllers (MKS).

All chemicals were thoroughly degassed prior to use. $PhSiH_3$ (Aldrich, 99%), Me_2O (Aldrich, >99.99%), Ar (BOC, >99.99%) and SF_6 (BOC, 99.9%) were used as supplied.

3. Experimental results

RRKM/master equation calculations performed for the SiH_2/Me_2O system have suggested that the high pressure limit for this reaction is reached at pressures in excess of 10^5–10^6 Torr.[14] To allow accurate extrapolations to determine the high-pressure limit rate constant, k_2^∞, it is desirable to undertake the kinetic measurements up to as high a total pressure as possible. The experiments were performed up to 850 Torr, the highest pressure attainable with our present apparatus. The SiH_2/Me_2O reaction was studied using two bath gases, SF_6 and Ar, and as expected the rate constants at a particular pressure are affected by the identity of the bath gas, although of course k_2^∞ should be independent of the bath gas. The maximum pressure achievable with SF_6 was lower than that for Ar and was limited by the range of flow rates attainable with the mass flow controllers.

3.1 Argon bath gas

The experimental observable is the SiH_2 relative concentration as a function of time following the photolysis laser pulse. A typical decay trace recorded at 294 K for SiH_2/Me_2O in Ar is shown in Fig. 1. Fits to such decay curves yield the pseudo-first-order rate constant, k_1, for the reaction.[23] Typical plots of k_1 *vs.* reactant pressure at a high and a low total pressure are shown in Fig. 2. Such plots give the second-order rate constant, k_2, at each total pressure.

At the highest temperature studied, 441 K, the decay traces collected at all total pressures (200–800 Torr) exhibited unusual behaviour, with both a fast and a slow component in the decay portion of the trace (see Fig. 3). The slow component extends over much longer times than would be associated with removal of SiH_2 by reaction with Me_2O, suggesting that there is a mechanism leading to replenishment of SiH_2 under these conditions. These decay traces were fitted with an exponential rise and double exponential decay to model the fast and slow components of the overall decay portion of the SiH_2 traces.

If the reaction involves the formation of an intermediate complex, the most straightforward mechanism for the observed behaviour at 441 K involves equilibrium being established between the reactants and the reaction complex. In such a mechanism there would be rapid initial decay of the SiH_2 concentration but as more of the complex is formed the rate of the reverse reaction increases and SiH_2 reforms through dissociation of the complex. The SiH_2 concentration would decay to a plateau at the equilibrium SiH_2 concentration. Another loss mechanism for SiH_2, such as reaction with another component of the mixture, diffusion from the obser-

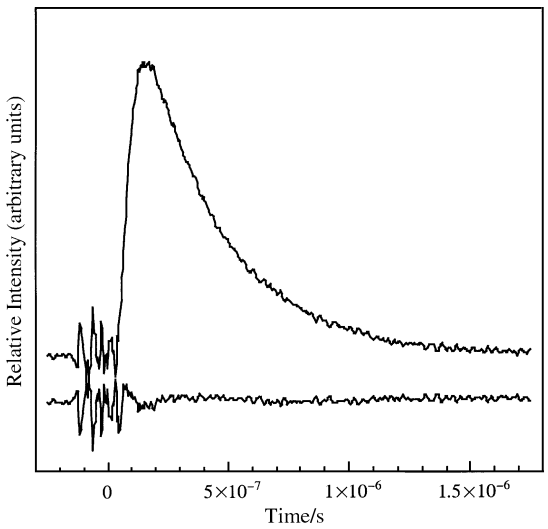

Fig. 1 Typical average decay trace for SiH_2 (10 mTorr of $PhSiH_3$ precursor) reacting with 0.5 Torr Me_2O at 400 Torr total pressure (Ar bath gas) and 294 K. The lower trace corresponds to the residuals from a biexponential fit.

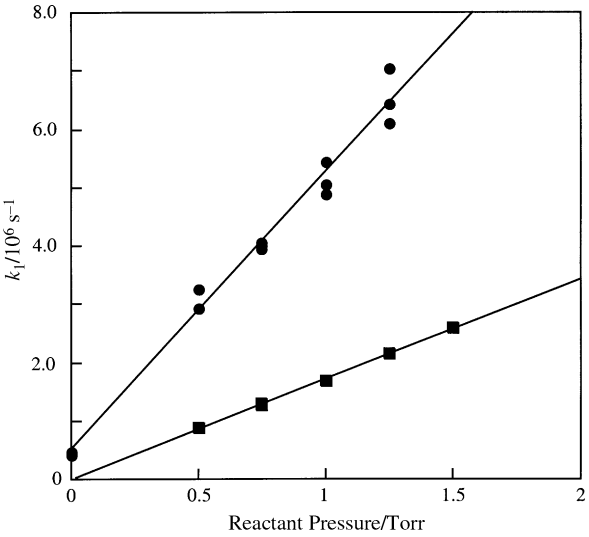

Fig. 2 Typical plots of the pseudo-first-order rate constants *vs.* reactant pressure for the reaction of SiH_2 with Me_2O. The data were obtained at total pressures of 600 Torr (circles) and 60 Torr (squares) at 294 K in Ar bath gas.

vation region, or reaction of the complex to form products, would then be responsible for the slow decay of the SiH_2 signal. Qualitatively, the observed SiH_2 time behaviour is consistent with this picture. The dissociation rate of the complex will increase with increasing temperature, and so the observation of this behaviour only at the highest temperature studied is consistent with the proposed explanation.

Kinetic models for this type of reaction scheme predict a double exponential decay in the SiH_2 concentration.[7] If a pre-equilibrium between reactants and complex is approached, the sum of the fast and slow rate constants, k_{fast} and k_{slow}, in this decay is related to the bimolecular rate constant, k_2, *via*

$$k_{fast} + k_{slow} = k_2[Me_2O] + c \quad (1)$$

where c is a constant. From the fits to the data, we find k_{slow} to be both small compared with k_{fast} and approximately constant with $[Me_2O]$, as we illustrate below. Thus

$$k_{fast} \cong k_2[Me_2O] + c' \quad (2)$$

where $c' = c - k_{slow}$ is constant. A plot of k_{fast} *vs.* $[Me_2O]$ yields the second-order rate constant, k_2, from the slope.

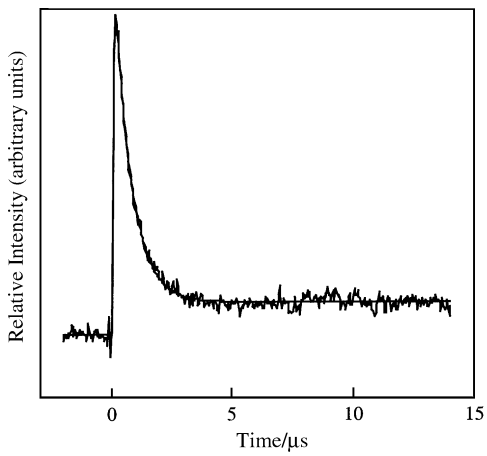

Fig. 3 Typical average decay trace for the high temperature (441 K) reaction of SiH_2 with Me_2O showing the raised baseline (10 mTorr $PhSiH_3$, 2.5 Torr Me_2O in 200 Torr total pressure of Ar buffer gas). The decay, which consists of 32 averages, is modelled with an exponential rise and double exponential decay.

Baggott *et al.*[7] have observed double exponential decay behaviour for $SiMe_2$ reacting with Me_2O, similar to our observations for SiH_2, and presented the appropriate kinetic scheme and expressions for the rate constants. The decay constants extracted should show certain dependencies on reactant concentration. k_{fast} should be linearly dependent on $[Me_2O]$ while k_{slow} should be independent of this variable. Our data conform to this expectation, as shown in Fig. 4. A further test is that $(Ak_{fast} + Bk_{slow})/(A + B)$, where A and B are the amplitudes of the fast and slow components respectively, is predicted to be independent of $[Me_2O]$. For $SiMe_2 + Me_2O$, Baggott *et al.* observed this term to be dependent on $[Me_2O]$, contrary to expectations. In the analysis of our data we find that the experimental uncertainties associated with the ratio $(Ak_{fast} + Bk_{slow})/(A + B)$, coupled with a smaller $[Me_2O]$ range in our experiments, prevent us from determining whether or not the ratio is dependent on $[Me_2O]$. However, we will demonstrate later that the pre-equilibrium model is consistent with the results of RRKM/master equation modelling and so eqn. (2) is expected to be relevant to our experiments. We believe it likely that a pre-equilibrium situation is also responsible for the experimental observations for the $SiMe_2 + Me_2O$ system, with the reason for Baggott's analysis not conforming with model expectations being the high fraction of Me_2O used, leading to this species playing a dual role of reactant and bath gas.

Rate constants for SiH_2 reacting with Me_2O have been obtained up to an Ar pressure of 850 Torr at four temperatures over the range 294–441 K (Table 1). The rate constants reported for 441 K are those extracted from the fast decay component of the overall decay trace, as discussed above. The rate constants clearly decrease with increasing temperature and increase with increasing pressure.

It is usual to extrapolate fall-off data to the high-pressure limit using a Lindemann–Hinshelwood form, or a modified version thereof. However, such extrapolations are only reliable when the data are near the high-pressure limit. Earlier RRKM calculations suggest that, even at the highest experimental pressures $\sim 10^3$ Torr, the reaction is a factor of $\sim 10^2$–10^3 below the high pressure limit.[14] Under these circumstances such extrapolation of the data will not provide a meaningful estimate of k_2^∞. RRKM/master equation modelling has been used to obtain the high-pressure Arrhenius parameters (see Section 4.2).

The negative temperature dependence seen in the data, *i.e.* the reduction in the rate constant with increasing temperature,

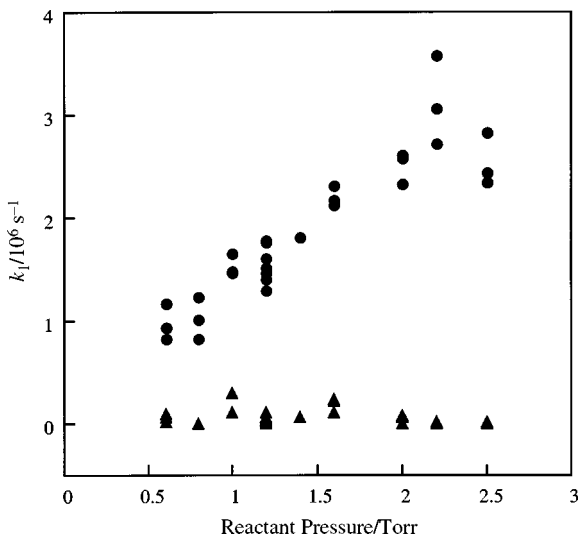

Fig. 4 k_{fast} (filled circles) and k_{slow} (filled triangles) variation with Me_2O pressure. The data are for total pressures of 600, 700 and 800 Torr in Ar bath gas.

Table 1 Second-order rate constants, k_2, for the reaction of SiH_2 with Me_2O at various temperatures and pressures (Ar bath gas)

	$k_2/10^{-11}$ cm^3 molecule^{-1} s^{-1}			
P/Torr	294 K	336 K	372 K	441 K
30	3.54 ± 0.1			
60	5.24 ± 0.04			
100	6.62 ± 0.1	4.40 ± 0.07	2.68 ± 0.19	
150	7.91 ± 0.3			
200	9.70 ± 0.3	6.40 ± 0.2	3.60 ± 0.18	2.30 ± 0.08
250	10.8 ± 0.4			
300	11.5 ± 0.1	7.90 ± 0.3	5.26 ± 0.16	
350	12.7 ± 0.7			
400	14.0 ± 0.6	9.56 ± 0.5	5.97 ± 0.14	3.24 ± 0.41
500	15.8 ± 0.9	10.4 ± 0.6	7.32 ± 0.67	
600	14.4 ± 0.5	11.4 ± 00.3	7.85 ± 0.43	4.37 ± 0.62
700	17.3 ± 0.7	12.1 ± 00.5	9.64 ± 0.58	4.25 ± 1.10
800	16.4 ± 0.8	13.5 ± 0.7	9.16 ± 0.52	5.25 ± 0.45
850	16.6 ± 0.8	13.4 ± 0.4		

is typical of the behaviour of systems involving the formation of an association complex.[28]

3.2 Sulfur hexafluoride bath gas

Results were obtained for the reaction of SiH_2 with Me_2O at 294 and 438 K using SF_6 as the bath gas (Table 2). SF_6 has no significant absorption at the photolysis wavelengths of 193 and 248 nm. The maximum pressure used in the SF_6 experiments was 150 Torr.

The SiH_2 decay traces are of similar quality to that shown in Fig. 1 for Ar bath gas and the plots of pseudo-first-order rate constants *vs.* reactant pressure are similar to Fig. 2. The SiH_2 decay traces at 438 K show the same raised baseline behaviour and fast and slow components as seen with Ar bath gas at 441 K. These decays were therefore treated in the same manner as described above for the Ar case to extract the second-order rate constants.

A comparison of the 294 K rate constants shows that those for SF_6 bath gas are approximately 1.4 times larger than the values for Ar bath gas at the same total pressure. The increased values for the rate constants arise from the increased collisional relaxation efficiency of the SiH_2–Me_2O complex by SF_6 compared to Ar. The rate constants obtained using both bath gases show a similar trend with total pressure. Our rate constants with SF_6 are uniformly lower than those reported by Becerra *et al.*,[14] with the difference being ~15% at 50 Torr.

3.3 Extraction of the equilibrium constant at 441 K

As we have noted in Section 3.1, the decay traces at 441 K display direct evidence for the formation of a pre-equilibrium. These decay traces can be fitted to extract the equilibrium constant for the system at this temperature. A direct experimental measurement of the equilibrium constant helps to constrain the later RRKM/master equation calculations through constraining the value of the critical energy for dissociation of the complex.

Table 2 Second-order rate constants, k_2, for the reaction of SiH_2 with Me_2O at 294 and 438 K at various pressures (SF_6 bath gas)

	$k_2/10^{-11}$ cm^3 molecule^{-1} s^{-1}	
P/Torr	294 K	438 K
30	4.66 ± 0.06	0.96 ± 0.07
60	7.25 ± 0.08	1.45 ± 0.11
100	9.19 ± 0.08	2.13 ± 0.09
150	10.99 ± 0.15	—

The reactions affecting the SiH_2 concentration can be modelled as:

$$SiH_2 + Me_2O \xrightarrow{k_f} SiH_2\text{–}Me_2O$$

$$SiH_2\text{–}Me_2O \xrightarrow{k_f} SiH_2 + Me_2O$$

$$SiH_2\text{–}Me_2O \xrightarrow{k_p} \text{products}$$

The reaction between SiH_2 and $PhSiH_3$ is not included as, due to the low concentration of $PhSiH_3$, its rate is much slower than that for the SiH_2/Me_2O reaction. k_p incorporates any process that removes the complex, and hence SiH_2. The SiH_2 concentration at any time is described by considering how the SiH_2 and SiH_2–Me_2O concentrations change with time:

$$\frac{d[SiH_2]_t}{dt} = -k_f[SiH_2]_t[Me_2O]_t + k_r[SiH_2\text{–}Me_2O]_t$$

$$\frac{d[SiH_2\text{–}Me_2O]_t}{dt} = k_f[SiH_2]_t[Me_2O]_t - k_r[SiH_2\text{–}Me_2O]_t - k_p[SiH_2\text{–}Me_2O]_t$$

where $[X]_t$ is the concentration of species X at time t. Under pseudo-first-order conditions, $[Me_2O]_t$ is constant and these equations reduced to:

$$\frac{d[SiH_2]_t}{dt} = -k_F[SiH_2]_t + k_r[SiH_2\text{–}Me_2O]_t$$

$$\frac{d[SiH_2\text{–}Me_2O]_t}{dt} = k_F[SiH_2]_t - (k_r + k_p)[SiH_2\text{–}Me_2O]_t$$

where $k_F = k_f[Me_2O]$, the t being omitted here as it is redundant.

These equations can be solved analytically or by numerical integration and fitted to the experimental decay curves. Over a short time period, Δt, they can be expressed as:

$$\Delta[SiH_2]_t = (-k_F[SiH_2]_t + k_r[SiH_2R]_t)\Delta t$$

$$\Delta[SiH_2R]_t = (k_F[SiH_2]_t - (k_r + k_p)[SiH_2R]_t)\Delta t = -\Delta[SiH_2]_t - k_p[SiH_2R]_t\,\Delta t$$

Since $[SiH_2]_{t+\Delta t} = [SiH_2]_t + \Delta[SiH_2]_t$ and $[SiH_2R]_{t+\Delta t} = [SiH_2R]_t + \Delta[SiH_2R]_t$, the concentration of each species is calculated from its concentration at the preceding time with a set of initial values, $[SiH_2]_0$ and $[SiH_2R]_0$, as input. The theoretical decay curves so obtained can be fitted to the experimental curves with k_F, k_r and k_p as variables. We have done this using a nonlinear least-squares fitting algorithm (Levenberg–Marquardt algorithm[29]). Since the experimental decay traces include the production of $SiH_2(0,0,0)$ (the rising portion), which is not a feature of the model discussed here, we fit the decays ignoring the first ~10% of the decay after time zero. Δt values were checked to ensure convergence.

A typical fit to a SiH_2/Me_2O decay is shown in Fig. 5. We find that the k_F values are consistent with those determined from the analysis of the experimental data discussed previously. The equilibrium constant, K_{eq}, can be obtained from

$$K_{eq} = \frac{k_f}{k_r} = \frac{k_F/[Me_2O]}{k_r}$$

K_{eq} should be independent of the total pressure at which the experiment is performed and hence also of the bath gas used.[30] The average value for K_{eq} determined from the Ar

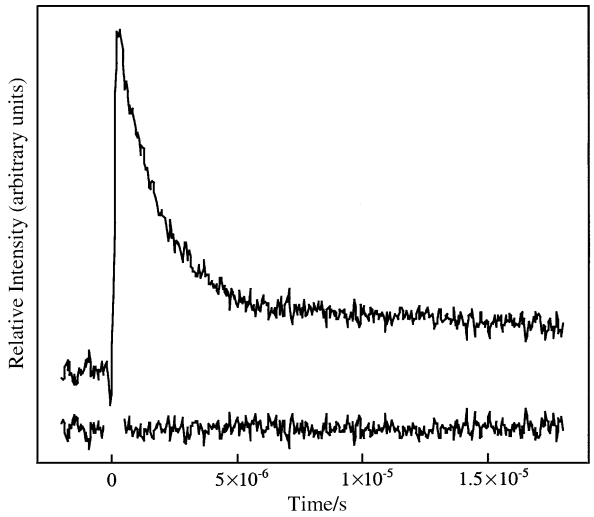

Fig. 5 A typical fit to a high temperature SiH_2 decay trace. The residuals (lower curve), which are the difference between the fit and the decay trace (upper curve), illustrate the quality of the fit. The SiH_2 decay trace was obtained under conditions of 1.0 Torr Me_2O and 200 Torr total pressure in Ar bath gas at a temperature of 441 K. The fit used Δt of 1×10^{-7} s and yielded k_F, k_r and k_p values of 5.06×10^5, 1.00×10^5 and 2.68×10^4 s^{-1}, respectively.

data is $2.2 \pm 0.7 \times 10^{-16}$ cm^3 $molecule^{-1}$ while that for the SF_6 data is $2.8 \pm 0.8 \times 10^{-16}$ cm^3 $molecule^{-1}$. Importantly, within the experimental uncertainty the equilibrium constant determined from the SF_6 data is the same as that determined from the Ar data.

The value for k_p was found to be ill-determined in the fitting and this rate constant could take any value below 10^4 s^{-1} without affecting how well the calculated curves fitted. This suggests that the process associated with k_p is slow and, coupling this with the results of the *ab initio* calculations which show a high barrier to rearrangement of the complex, we suggest that the slow decay of SiH_2 is associated with its diffusion from the volume interrogated by the laser and/or its reaction with other species rather than subsequent reaction of the complex.

Having a value for K_{eq} provides a check for the RRKM/master equation calculations that are presented later, in particular the value of the critical energy, E_0. Since the reaction of interest involves a barrierless recombination, K_{eq} is related to E_0 *via*[30]

$$K_{eq} = \frac{Q^{tr}_{AB}}{Q^{tr}_{A} Q^{tr}_{B}} \frac{Q'_{AB}}{Q'_{A} Q'_{B}} \exp\left(\frac{E_0}{k_B T}\right)$$

Here Q^{tr}_{A}, Q^{tr}_{B} and Q^{tr}_{AB} are the translational partition functions, while Q'_{A}, Q'_{B} and Q'_{AB} are the product of the electronic, vibrational and rotational partition functions. The value of K_{eq} thus depends exponentially on E_0. Using parameters determined from *ab initio* calculations (see the following section) to calculate the partition functions, an E_0 value consistent with the experimentally determined K_{eq} can be calculated. With this approach we determine E_0 to be 88.4 ± 1.7 kJ mol^{-1}.

4. Modelling the SiH_2/Me_2O system

The pressure and temperature dependence of the rate constants have been modelled using an RRKM/master equation approach. This determines the rate for the $SiH_2 + Me_2O$ reaction from that for the unimolecular dissociation of the SiH_2–Me_2O complex. *Ab initio* calculations have been used to supply the necessary input data for the RRKM calculations. These calculations were performed for the SiH_2–Me_2O complex and its constituents (SiH_2 and Me_2O) using the GAUSSIAN suite of programs.[31] The calculations for SiH_2 and Me_2O allow a comparison of the calculated frequencies with experimental values, thereby providing a check of their accuracy, and also allow the stabilisation energy of the complex to be determined.

4.1 *Ab initio* calculations

The initial geometry of each complex and reactant was found using Hartree–Fock (HF) theory with a minimal basis set (HF/6-31G**) and then refined with increasing complexity of theory and basis set until the calculations were performed with the final theory/basis set, MP2/6-311+G**. The harmonic vibrational frequencies were scaled by the recommended factor of 0.9496 before use in the statistical mechanical calculation of thermodynamic quantities and the RRKM calculations.[32] No imaginary frequencies were found for any of the structures, indicating that they correspond to local minima on the relevant potential energy surfaces. A comparison of the scaled MP2/6-311+G** vibrational frequencies for SiH_2 and Me_2O with experimental values shows that they lie within a few percent of each other.

The calculations show that an association complex forms between SiH_2 and Me_2O. A representation of the complex geometry is shown in Fig. 6. The geometry of the two halves of the SiH_2–Me_2O complex are much the same as in the fragments SiH_2 and Me_2O. Key features are (i) Si–H bond length = 0.1515 nm, (ii) Si–O bond length = 0.203 nm, Si–O–C angle = 111.38° and H–Si–O angle = 87.9°. The H–Si–O angle is, as expected, based on an interaction between the p-orbital of the Si atom and the lone pair on the O atom. The calculated Si–O bond length is longer than those found in stable molecules. The reactant molecule is positioned perpendicular to the H–Si–H plane, in keeping with SiH_2 accepting electron density into an empty p-orbital, which lies perpendicular to the H–Si–H plane.

The calculations show the electronic energy of the complex to be stabilized by 97.2 kJ mol^{-1} compared with the reactants and the difference in zero point energies, determined using scaled *ab initio* harmonic frequencies, is 82.9 kJ mol^{-1}. This is slightly lower than the value of 84.3 kJ mol^{-1} recently reported by Heaven *et al.*,[33] whose calculations used a basis set with more diffuse functions because of their desire to compare the behaviour of silylene with that of germylene. While this is much lower than a typical chemical bond, it nevertheless indicates that a significant bond is formed between the two moieties. It is comparable, for example, to the critical energy for dissociation of the propyl radical to form a methyl radical and ethylene.[34] The value of 82.9 kJ mol^{-1} compares favourably with the value of 88.4 ± 1.7 kJ mol^{-1} determined from the high-temperature equilibrium constant.

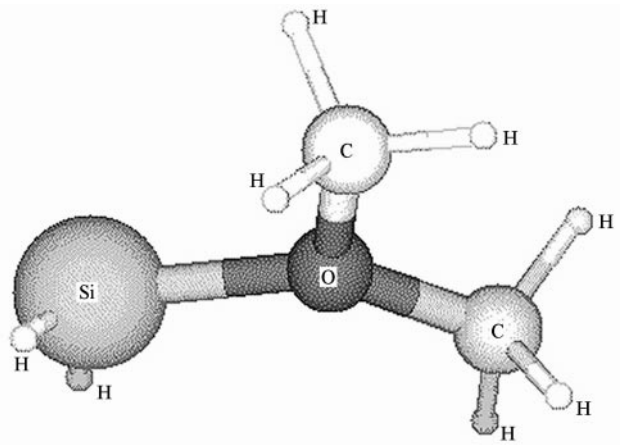

Fig. 6 A representation of the MP2/6-311+G** optimised geometry of the SiH_2–Me_2O complex.

Calculations of the $SiH_2 + Me_2O$ system recently reported by Heaven *et al.*[33] have explored the reaction pathways beyond the complex. They find the barrier to further reaction of the complex to be significant (193.3 kJ mol^{-1}). At the temperatures of our experiment there is thus no possibility of further reaction of the complex other than the channel leading back to SiH_2 and Me_2O. These *ab initio* predictions for SiH_2–Me_2O are consistent with experiments for the methylated analogue of SiH_2, $SiMe_2$, which shows rearrangement products for alcohols but not for Me_2O.[7,35]

4.2 RRKM/master equation modelling

The SiH_2–Me_2O fission and SiH_2/Me_2O association reactions are described as:

$$SiH_2 + Me_2O \underset{k_2}{\overset{k_{-2}}{\rightleftharpoons}} SiH_2\text{–}Me_2O$$

The bimolecular rate constant, k_2, is related to the unimolecular rate constant, k_{-2}, *via* the reaction equilibrium constant, $K_{eq} = k_2/k_{-2}$. RRKM/master equation calculations were carried out using the UNIMOL program suite[36] to obtain k_{-2} values for total pressures ranging over those covered experimentally and up to the high-pressure limit. K_{eq} is determined in the usual manner from the partition functions and enthalpy difference between reactants and products at 0 K[37] (see Section 3.3 above). The bimolecular rate constant is then calculated from k_{-2} and K_{eq}.

The RRKM calculations are performed using the Gorin model, which has been extensively used for simple bond fission reactions producing fragments that do not show extensive electronic rearrangement (resonance stabilization). In this transition state model, the stretch in the breaking bond is assigned as the reaction coordinate, the torsion around that bond becomes a free rotation, and the four bending modes that are destined to become external rotations of the products are weakened. The internal modes of this "loose" transition state are simply the vibrations and rotations of the independent product fragments, and the four low-frequency bending modes associated with the breaking bond are considered to be two two-dimensional internal rotations of the product fragments that are hindered by some angular potential function. The extent to which a fragment rotation in the transition state is hindered due to the presence of the other fragment is accounted for by reducing the moment of inertia of the free rotor to an "effective" moment of inertia for the hindered rotor as determined by the hindrance angle.

The input parameters for the RRKM/master equation calculations are based largely on the results of the *ab initio* calculations. Having multiple temperature data was found to provide a tight constraint on the fitting parameters. The variable parameters in our approach are $r^{\dagger}$, the Si–O bond length in the transition state, E_0, the critical energy, and the lowest frequency of the transition state. For the SiH_2–Me_2O complex, the Si–O bond stretch (*ca.* 440 cm^{-1}) was selected as the reaction coordinate, and this bond was lengthened from a ground-state value of 0.230 nm to a transition-state value, $r^{\dagger} = 0.400$–0.525 nm, depending on the temperature. The values used were 0.4, 0.45, 0.47 and 0.525 nm at temperatures of 441, 372, 336 and 294 K, respectively. The transition state becomes tighter as the temperature is increased. With $r^{\dagger} = 0.525$ nm at 294 K, $A_{-2,\infty} = 10^{17.30}$ s^{-1}, a value within an acceptable range for simple fission reactions (16 to 17.5).[30]

The Si–O torsional motion was treated as a low frequency vibration since treating it as a rotational motion leads to poor fits to the pressure-dependent data because there is too high an entropy in the transition state. Two C–O–Si bends and two H–Si–O bends associated with the breaking Si–O bond were replaced by two-dimensional rotors. Calculations using the alternate approach where low-frequency rocking vibrations are used instead of two-dimensional rotations did not reproduce the experimental behaviour. Consideration of steric hindrance between the fragments was not necessary in this model due to the lack of bulky fragments and the relatively long Si–O bond length. The external moment of inertia that corresponds to rotation about the Si–O axis was treated as active in both the molecule and the transition state. A vibrational assignment and the structural and thermodynamic properties for the SiH_2–Me_2O complex were obtained from the *ab initio* calculations. The molecular parameters used in the RRKM calculations are listed in Table 3.

In the master equation calculations an exponential-down model for the energy transfer was employed:

$$P(E, E') = \frac{1}{N(E')} \exp\left[-\left(\frac{E' - E}{a}\right)\right], \quad (E < E')$$

where E' and E are the reactant energies before and after a collision, respectively, $N(E')$ is a normalising factor and α is a parameter related to the average downward energy transferred per collision, $\langle \Delta E_{down} \rangle$. The value for $\langle \Delta E_{down} \rangle$ is the only parameter varied in the master equation calculations. For Ar, Becerra *et al.*[38] found a constant value of 300 cm^{-1} applied over the range 298–665 K for the pressure dependence of SiH_2 reactions. This is consistent with values in the range 260–350 cm^{-1} at room temperature obtained from various kinetic and energy transfer studies.[30] Values of $\langle \Delta E_{down} \rangle$ for SF_6 in SiH_2 reaction systems have been found to range from ~800 to 1000 cm^{-1} over the temperature range 298 to ~500 K and from ~700 to 900 cm^{-1} between ~500 and 650 K.[38–40] Based on these previous studies, we have applied temperature-independent $\langle \Delta E_{down} \rangle$ values for SF_6 in the range 650–750 cm^{-1} and for Ar in the range 300–350 cm^{-1}. It was found that varying the $\langle \Delta E_{down} \rangle$ value over these ranges had only a small effect on the predicted bimolecular rate constants.

Fig. 7 shows the calculated fall-off curves with the experimental data for Ar bath gas, while Fig. 8 shows the calculated curves extrapolated to the high-pressure limit. Fig. 9 illustrates the corresponding fit for the SF_6 experimental data. The high-pressure limit rate constant, k_2^{∞}, occurs at a total pressure of ~10^7 Torr. Our experimental data were obtained at pressures below 10^3 Torr. The data are thus extrapolated to the high-pressure limit over four orders of magnitude. The calculated fall-off curves predict that the temperature dependence of the rate constants switches at ~10^5 Torr from being negative below this pressure to being positive above it. The log A_{-2} and k_2^{∞} values calculated at each temperature are given in Table 4. An Arrhenius plot of k_2^{∞} yields the following param-

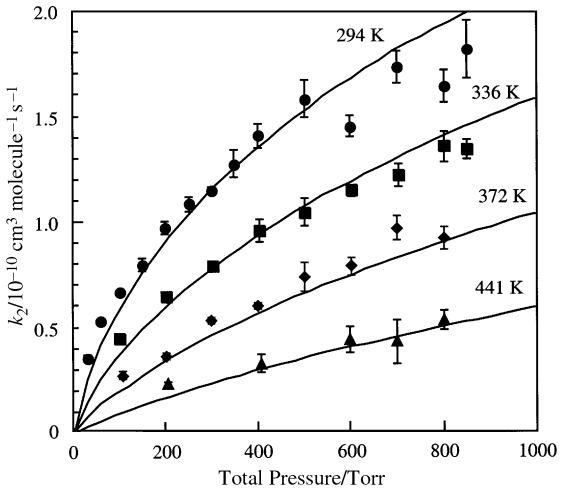

Fig. 7 The pressure-dependent second-order rate constants for the SiH_2/Me_2O reaction in Ar bath gas at 294 (filled circles), 336 (filled squares), 372 (filled diamonds) and 441 K (filled triangles) fitted with the RRKM/master equation analysis (lines).

Table 3 RRKM parameters for the decomposition of the SiH_2–Me_2O complex

	Reactant	Transition state
Frequencies/cm^{-1}	3074	3026
	3062	3025
	3012	2937
	3010	2931
	2924	2877
	2920	2869
	2015	2049
	1960	2044
	1453	1465
	1443	1446
	1435	1435
	1428	1433
	1426	1425
	1400	1409
	1226	1220
	1162	1166
	1141	1153
	1121	1121
	1042	1084
	974	1014
	885	922
	752	401
	704	249
	440	200
	293	200
	258	
	248	
	189	
	163	
	109	
Rotational constants/cm^{-1} [a]		
Inactive external	0.109(1,2)	0.028(1,2)
Active external	0.292(1,1)	0.292(1,1)
Internal		
SiH_2		7.602(1,2)[b]
Me_2O		0.321(2,2)[b]
log (A_∞/s^{-1}) at 294 K		17.3
Path degeneracy		1.0
Critical energy, E_0/kJ mol^{-1}		87.0
Lennard-Jones parameters	σ_{LJ}, ε_{LJ}	3.9, 164 (Ar bath gas)
		4.7, 252 (SF_6 bath gas)

[a] Quantities in parentheses are symmetry number and dimension, respectively. [b] Rotational constants for $r^\dagger = 0.525$ nm.

eters: log (A/cm^3 $molecule^{-1}$ s^{-1}) = -7.6 ± 0.4 and $E_a = 9.3 \pm 2.8$ kJ mol^{-1}.

It is important to note that one does not obtain a unique set of parameters from the RRKM/master equation fits. For

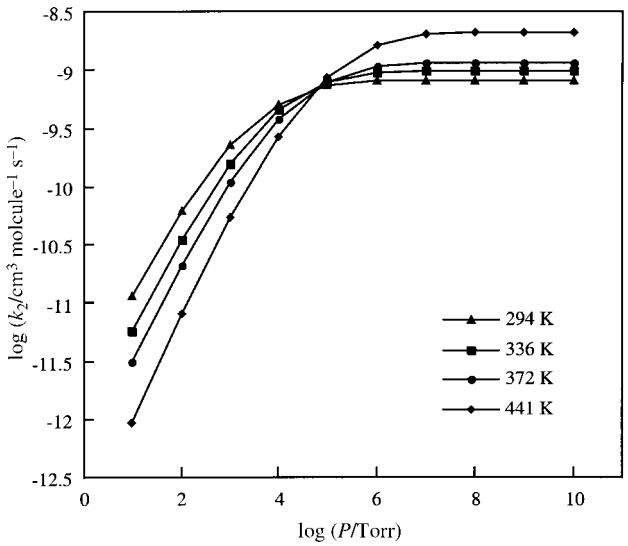

Fig. 8 A plot of the pressure dependence of the rate constants calculated from the RRKM/master equation fit to the data shown in Fig. 7.

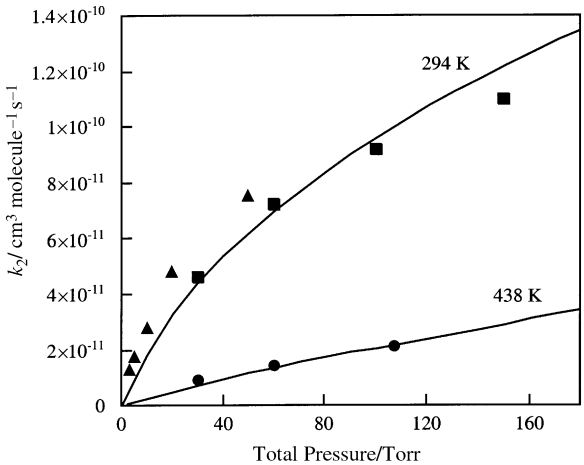

Fig. 9 RRKM/master equation fit to experimental rate constants obtained for the SiH_2/Me_2O reaction in SF_6 bath gas at temperatures of 294 (filled circles) and 438 K (filled squares). The RRKM parameters are those optimised to fit the data for Ar bath gas with changes to the Lennard-Jones collision parameters and $\langle E_{down} \rangle$ appropriate for SF_6. A $\langle E_{down} \rangle$ value of 700 cm^{-1} was used. The error bars for the experimental data are smaller than the symbols shown. The results (filled triangles) of Becerra *et al.*[14] at 296 K are shown for comparison.

Table 4 Log A_{-2} and k_2^{∞} values determined from the RRKM/master equation fits to the experimental data at each of the temperatures studied

Temperature/K	294	336	372	441
log (A_{-2}/s^{-1})	17.30	17.19	17.12	16.96
k_2^{∞}/cm^3 molecule^{-1} s^{-1}	8.09×10^{-10}	1.02×10^{-9}	1.14×10^{-9}	2.13×10^{-9}

example, we find that the E_0 value could vary from 85.4 to 87.0 kJ mol^{-1} (with, of course, compensating changes in the other parameters) with similar quality fits obtained. While a $\langle \Delta E_{down} \rangle$ value for Ar of 320 cm^{-1} was used in the calculations, we find that values in the range 300–350 cm^{-1} give similar results. At 441 K, the calculated K_{eq} is 1.9×10^{-16} cm^3 molecule^{-1}. This compares with the experimentally determined values of $2.2 \pm 0.7 \times 10^{-16}$ cm^3 molecule^{-1} and $2.8 \pm 0.8 \times 10^{-16}$ cm^3 molecule^{-1} with Ar and SF_6 as the collision partners, respectively.

5. Discussion

The SiH_2/Me_2O reaction is expected to be similar to the $SiMe_2$/Me_2O reaction. For the $SiMe_2$/Me_2O reaction, both C–H and C–O bond insertion is possible but no reaction products corresponding to C–O bond insertion have been observed[7,8] and C–H insertion is unlikely.[9,10] *Ab initio* calculated reaction profiles[34] show that rearrangement of the SiH_2–Me_2O complex has too high an energy barrier to occur with our experimental conditions. The previous experimental study of the SiH_2/Me_2O reaction provided evidence for reaction involving the formation of a stabilized SiH_2–Me_2O complex as the only product.[14]

Our data provide further support for this. The negative temperature dependence observed for the experimentally measured SiH_2/Me_2O second-order rate constants is the reverse of the expected behaviour for most simple reactions. The negative temperature dependence and the total pressure dependence of the rate constants combine to reinforce the presence of a complex mechanism. Particularly important is the observation of decays that do not return to the baseline at elevated temperatures (~440 K) as this is direct evidence for complex formation and subsequent decay. The slow decay of these curves to the baseline provides direct evidence for the longevity of the complex. Analysis of these high-temperature decay curves allows the equilibrium constant to be determined. This has provided an experimental measurement for the well-depth of the complex. Behaviour similar to that seen in our elevated temperature work has been seen for the analogous reactions of $SiMe_2$ with Me_2O[7] and the cyclic ether, tetrahydrofuran[8] at lower temperatures, and with CH_3OH at temperatures >421 K.[10]

The well-depth determined from the RRKM/master equation fits to the data is 87 kJ mol^{-1}. This compares well with the values calculated by *ab initio* methods (82.9 kJ mol^{-1})[34] and from the experimentally determined 441 K equilibrium constant (88.4 ± 1.7 kJ mol^{-1}). This value is, however, somewhat lower than the value of 96 kJ mol^{-1} determined in our previous fit to a more limited data set.[14] The availability of the fall-off data at elevated temperatures has provided a constraint that was absent in the earlier analysis. We noted previously that E_0 was poorly constrained with a set of data at a single temperature. Note also that the value of $10^{17.7}$ s^{-1} at 294 K for $A_{-2,\infty}$ calculated previously is higher than the value of $10^{17.30}$ s^{-1} obtained here from the current set of molecular and transition state parameters so the values for E_0 would be in much closer agreement for the same value of $A_{-2,\infty}$.

The rate constants obtained with SF_6 bath gas in the present work are consistently lower than those reported previously. We note that the new data provide a better match with the RRKM/master equation analysis than did the previous data. For this reason we believe the present data to be more reliable than those presented previously.

The high-pressure limit values for the rate constants as determined by the RRKM/master equation calculations are highly unusual. An issue with the analysis is the large pressure range over which the data are extrapolated to the high-pressure limit. Because fall-off curves approach the high-pressure limit asymptotically, we quote pressure values for which k_2/k_2^{∞} is 0.9. k_2/k_2^{∞} is predicted to be 0.9 at pressures of 1×10^5, 3×10^5, 6×10^5 and 5×10^6 Torr at temperatures of 294, 336, 372 and 441 K, respectively. Thus the extrapolation to the high-pressure region is over ~2–3 orders of magnitude in pressure. Consequently, it is likely that the high-pressure rate constants and the pressure values required to reach this limit are not reliable. Nevertheless, the fact that the calculations produce such an unusual set of values leads to the question of whether there are unusual features of the system that might lead to it having behaviour that differs from the norm.

Trends that are a consistent feature of the RRKM calculations using a wide variety of parameters are: (i) the high-pressure limit is reached at unusually high pressure (*e.g.*, the values obtained here compare with 10^5 Torr in ref. 14); (ii) the reaction is very efficient, with indications that the high-pressure limit rate constant is larger than the Lennard-Jones collision rate constant (for comparison, the high-pressure rate constant for the $^1CH_2$/Me_2O reaction is ~1/3 of the Lennard-Jones collision rate constant[41]); (iii) in the high-pressure limit the reaction is predicted to have a positive temperature dependence over the range studied, indicating a barrier to reaction. We have examined the system to explore why it is displaying this unusual behaviour and, therefore, when such unusual behaviour might be found in other systems.

The high-pressure limit for the rate constant corresponds to the situation where collisions can rapidly repopulate levels depleted by reaction and hence there is a steady-state population in the levels above dissociation. The larger the microscopic rate constants for dissociation, the higher the pressure required to reach the high-pressure limit because the collisional energy transfer rate constants must exceed the dissociation rate constants at the high-pressure limit. A very high-pressure value required to reach for the high-pressure limit thus implies unusually large microscopic rate constants for unimolecular dissociation of the complex. The microscopic rate constants, $k(E)$, are given by RRKM theory as:[30]

$$k(E) = \frac{\int_0^{E-E_0} \rho^{\dagger}(E_+)\,dE_+}{h\rho(E)}$$

Here $\rho^{\dagger}(E_+)$ is the density of states of the transition state at energy E_+ above the critical energy E_0, $\rho(E)$ is the density of states of the molecular reactant and h is Planck's constant. Since the vibrational frequencies of the complex are not particularly unusual, the density of states will increase in the usual way. However, a key difference between the complex and the more usual unimolecular dissociations is the very low critical energy for dissociation. Thus, while the numerator in the RRKM rate constant expression is expected to vary with increasing energy in a manner analogous to that for usual

systems, the denominator will be much smaller than usual due to the lower energy (associated with the smaller value for E_0). This leads to the $k(E)$ values being unusually large, and it therefore follows that an unusually high value for the high-pressure limit is required.

In this context it is interesting to compare the values for $k(E)$ in the SiH_2/Me_2O system to those for other, more typical systems. Consider, for example, the thermal decomposition of phenylsilane, $PhSiH_3$ which has been studied by O'Neal *et al.*[42] This system has an E_0 for dissociation into PhSiH and H_2 of 257 kJ mol^{-1} and at 1150 K a value of k_2/k_2^∞ of 0.9 is reached at ~50 Torr total pressure. The contribution to the dissociation rate of particular $k(E)$ values can be estimated by examining the function $k(E)\ \rho(E)\exp(-E/kT)$, where $\rho(E)$ is the density of states at energy E. Using the RRKM parameters reported by O'Neal *et al.* it can be determined that this function peaks at 13 000 cm^{-1} above the critical energy and falls to 50% of the peak at 18 100 cm^{-1} above E_0, 20% at 21 400 cm^{-1} above E_0 and 10% at 23 200 cm^{-1} above E_0. The corresponding $k(E)$ values are 1.5×10^6, 1.8×10^7, 6.4×10^7 and 1.2×10^8 s^{-1}. The comparable values for the SiH_2/Me_2O system at 294 K are as follows. The function $k(E)\ \rho(E)\exp(-E/kT)$ peaks at 2700 cm^{-1} above E_0, where $k(E)$ is 4.0×10^9 s^{-1}, drops to 50% by 3400 cm^{-1} above E_0 where $k(E)$ is 2.5×10^{10} s^{-1}, to 20% by 3900 cm^{-1} above E_0 where $k(E)$ is 6.0×10^{10} s^{-1} and to 10% by 4200 cm^{-1} where $k(E)$ is 9.4×10^{10} s^{-1}. At comparable points in the function the $k(E)$ values for SiH_2/Me_2O are ~1–2 $\times 10^3$ larger than they are for $PhSiH_3$ decomposition. We thus expect the high-pressure limit to be reached at pressures ~1–2 $\times 10^3$ larger than is the case for $PhSiH_3$ decomposition, *i.e.* k_2/k_2^∞ should be 0.9 at pressures of ~5 $\times 10^4$ to 1 $\times 10^5$ Torr. At 294 K k_2/k_2^∞ is 0.9 at 1 $\times 10^5$ Torr. This comparison illustrates that the high pressures required to reach the high-pressure limit for SiH_2/Me_2O are a straightforward consequence of the $k(E)$ values being unusually large in this system.

The analysis presented above suggests that large high-pressure limit pressures will be a general feature of systems with unusually low E_0 values. Hippler and co-workers have recently reported the results of an extensive series of studies of the unimolecular decomposition of alkoxyl radicals.[43,44] These species have relatively low E_0 values. The recent work concerns the isopropoxyl radical and includes data up to very high pressures (~5 $\times 10^4$ Torr).[43] E_0 for this system is 63.7 kJ mol^{-1}. At 330 K the experimental rate constants reach 90% of the high-pressure limit value reported by the authors at 2 $\times 10^4$ Torr. At 408 K the rate constant at the highest pressure for which data are available (4.6 $\times 10^4$ Torr) is only 77% of the high-pressure limit. This suggests that the 90% value is in the 10^5–10^6 Torr range. The isopropoxyl radical system which, like SiH_2–Me_2O, has a low E_0 value, thus has high-pressure limit values similar to those reported here for the SiH_2/Me_2O system, consistent with our expectations based on the analysis above.

A high efficiency for the reaction implies that it involves a long-range attraction between the reactant species. This appears to be a consequence of the large Si–O bond length in the transition state. The collision diameter that is used for the calculation of Lennard-Jones collision frequencies is 0.42 nm. The Si–O separation in the transition state places the SiH_2 and Me_2O further apart than this (~0.50 nm).

The calculations suggest that the rate constants revert to the usual positive temperature dependence in the high-pressure limit, *i.e.*, they increase with increasing temperature. The recombination reaction occurs on an effective potential that is the sum of the intermolecular potential (approximated as a one dimensional Morse oscillator in the RRKM calculations) and a "centrifugal potential" associated with the orbital angular momentum of the approaching reactants.[30] The centrifugal term can act to set up a barrier to reaction. We have calculated the value of the centrifugal term and the potential energy term at the transition state positions at each temperature for an impact parameter corresponding to the transition state bond length. The potential is taken to be a Morse function with the same parameters as used for the RRKM calculations. The results of these calculations are given in Table 5.

The feature that emerges from this calculation is that for the 294 to 372 K data the centrifugal barrier height exceeds the decrease in the potential energy at the transition state, the net result being a barrier between reactants and the association product. As the temperature increases this barrier height is reduced as the transition state moves in tighter and the decrease in potential energy becomes much larger. As the temperature increases eventually the decrease in the potential energy at the transition state more than offsets the increase due to the centrifugal term and overall there is no barrier, as we see in the calculations for 441 K. The presence of a barrier will cause the rate to increase with increasing temperature over the range of our experiments. While these calculations are only indicative, they show that for a shallow well the effect of the centrifugal term can be considerable. A key feature is that the decrease in the potential energy at the transition state is small and a barrier will also result with smaller values of the impact parameter.

The unusual temperature dependence appears to arise because the SiH_2–Me_2O bond is unusually weak and this is coupled with the transition state being at large separation where the potential energy is not much reduced from the asymptotic value. The weak bond and large separation mean that the centrifugal term can become important by creating a barrier at low temperatures, leading to a positive temperature dependence in this temperature regime. It is readily shown by repeating the calculations of potential energy and centrifugal barrier height for a system with a more typical dissociation energy that the total energy is now negative over the full temperature range of the experiment. Thus, at more typical values of the dissociation energy there is no barrier since the centrifugal term is now smaller than the decrease in the potential energy at the transition state. This will also be the situation where the well-depth is shallow but the transition state is at smaller separations than for the SiH_2/Me_2O case.

As we discussed above, the weak bond was also responsible for making the pressure dependence unusually high. A prediction of our analysis is that similarly weakly bonded systems will show unusual pressure and temperature behaviour.

Table 5 The values of the centrifugal and potential energy terms at the transition state positions at each temperature for an impact parameter corresponding to the transition state bond length. The potential is a Morse function with the same parameters as used for the RRKM calculations

Temperature/K	294	336	372	441
Transition state bond length/nm	0.525	0.47	0.45	0.40
Centrifugal energy/cm^{-1}	258	295	327	387
Potential energy/cm^{-1}	−47	−125	−178	−430
Total energy/cm^{-1}	211	170	149	−43

Acknowledgements

This work was supported in part by the Australian Research Council. UNA acknowledges the financial support provided by an Australian Postgraduate Award. The help of the Mechanical, Glassblowing and Engineering Workshop staff at Flinders University is gratefully acknowledged. We thank Professor Robin Walsh for helpful correspondence.

References

1 J. M. Jasinski, B. S. Meyerson and B. A. Scott, *Annu. Rev. Phys. Chem.*, 1987, **38**, 109.
2 P. P. Gaspar, in *Reactive Intermediates*, ed. M. Jones, Jr. and R. A. Moss, Wiley, New York, 1978, vol. 1, p. 229.
3 P. P. Gaspar, in *Reactive Intermediates*, ed. M. Jones, Jr. and R. A. Moss, Wiley, New York, 1981, vol. 2, p. 335.
4 P. P. Gaspar, in *Reactive Intermediates*, ed. M. Jones Jr. and R. A. Moss, Wiley, New York, 1985, vol. 3, p. 333.
5 G. Inoue and M. Suzuki, *Chem. Phys. Lett.*, 1985, **122**, 361.
6 J. E. Baggott, M. A. Blitz, H. M. Frey, P. D. Lightfoot and R. Walsh, *Chem. Phys. Lett.*, 1987, **135**, 39.
7 J. E. Baggott, M. A. Blitz and P. D. Lightfoot, *Chem. Phys. Lett.*, 1989, **154**, 330.
8 J. E. Baggott, M. A. Blitz, H. M. Frey, P. D. Lightfoot and R. Walsh, *Int. J. Chem. Kinet.*, 1992, **24**, 127.
9 J. M. Jasinski, R. Becerra and R. Walsh, *Chem. Rev.*, 1995, **95**, 1203.
10 R. Becerra and R. Walsh, in *Research in Chemical Kinetics*, ed. R. G. Compton and G. Hancock, Elsevier, Amsterdam, 1995, vol. 3.
11 N. Al-Rubaiey and R. Walsh, *J. Phys. Chem.*, 1994, **98**, 5303.
12 R. Becerra and R. Walsh, *Int. J. Chem. Kinet.*, 1994, **26**, 45.
13 G. J. Gutsche, PhD Thesis, The Flinders University of South Australia, 1997.
14 R. Becerra, I. W. Carpenter, G. J. Gutsche, K. D. King, W. D. Lawrance, W. S. Staker and R. Walsh, *Chem. Phys. Lett.*, 2001, **333**, 83.
15 K. Raghavachari, J. Chandrasekhar, M. S. Gordon and K. J. Dykema, *J. Am. Chem. Soc.*, 1984, **106**, 5853.
16 S. Su and M. S. Gordon, *Chem. Phys. Lett.*, 1993, **204**, 306.
17 W. S. Staker, K. D. King, G. J. Gutsche and W. D. Lawrance, *J. Chem. Soc., Faraday Trans.*, 1991, **87**, 2421.
18 W. S. Staker, K. D. King, G. J. Gutsche and W. D. Lawrance, *J. Chem. Soc., Faraday Trans.*, 1992, **88**, 659.
19 F. J. Hayes, G. J. Gutsche, W. D. Lawrance, W. S. Staker and K. D. King, *Combust. Flame*, 1995, **100**, 653.
20 F. Hayes, W. D. Lawrance, W. S. Staker and K. D. King, *J. Phys. Chem.*, 1996, **100**, 11314.
21 F. J. Hayes, W. D. Lawrance, W. S. Staker and K. D. King, *Chem. Phys. Lett.*, 1994, **231**, 530.
22 M. A. Buntine, G. J. Gutsche, W. S. Staker, M. W. Heaven, K. D. King and W. D. Lawrance, *Z. Phys. Chem.*, in the press.
23 U. N. Alexander, N. A. Trout, K. D. King and W. D. Lawrance, *Chem. Phys. Lett.*, 1999, **299**, 291.
24 U. N. Alexander, K. D. King and W. D. Lawrance, *Chem. Phys. Lett.*, 2000, **319**, 529.
25 J. M. Jasinski and J. O. Chu, *J. Chem. Phys.*, 1988, **88**, 1678.
26 H. Ishikawa and O. Kajimoto, *J. Phys. Chem.*, 1994, **98**, 122.
27 J. O. Chu, D. B. Beach and J. M. Jasinski, *J. Phys. Chem.*, 1987, **91**, 5340.
28 J. Troe, *J. Chem. Soc., Faraday Trans.*, 1994, **90**, 2303.
29 W. H. Press, B. P. Flannery, S. A. Teukolsky and W. T. Vetterling, *Numerical Recipes: The Art of Scientific Computing* (*Fortran Version*), Cambridge University Press, Cambridge, 1989.
30 R. G. Gilbert and S. Smith, *Theory of Unimolecular and Recombination Reactions*, Blackwell Scientific Publications, Oxford, 1990.
31 *GAUSSIAN 98*, *Revision A.7*, M. J. Frisch, G. W. Trucks, H. B. Schlegel, G. E. Scuseria, M. A. Robb, J. R. Cheeseman, V. G. Zakrzewski, J. A. Montgomery, Jr., R. E. Stratmann, J. C. Burant, S. Dapprich, J. M. Millam, A. D. Daniels, K. N. Kudin, M. C. Strain, O. Farkas, J. Tomasi, V. Barone, M. Cossi, R. Cammi, B. Mennucci, C. Pomelli, C. Adamo, S. Clifford, J. Ochterski, G. A. Petersson, P. Y. Ayala, Q. Cui, K. Morokuma, D. K. Malick, A. D. Rabuck, K. Raghavachari, J. B. Foresman, J. Cioslowski, J. V. Ortiz, A. G. Baboul, B. B. Stefanov, G. Liu, A. Liashenko, P. Piskorz, I. Komaromi, R. Gomperts, R. L. Martin, D. J. Fox, T. Keith, M. A. Al-Laham, C. Y. Peng, A. Nanayakkara, C. Gonzalez, M. Challacombe, P. M. W. Gill, B. Johnson, W. Chen, M. W. Wong, J. L. Andres, C. Gonzalez, M. Head-Gordon, E. S. Replogle and J. A. Pople, Gaussian, Inc., Pittsburgh, PA, 1998.
32 A. P. Scott and L. Radom, *J. Phys. Chem.*, 1996, **100**, 16505.
33 M. W. Heaven, G. F. Metha and M. A. Buntine, *J. Phys. Chem. A*, 2001, **105**, 1185.
34 H. E. O'Neal and S. W. Benson, *Kinetic Data on Gas Phase Unimolecular Reactions*, NSRDS-NBS21, National Bureau of Standards, Washington, DC, 1970.
35 K. P. Steele and W. P. Weber, *Inorg. Chem.*, 1981, **20**, 1302.
36 R. G. Gilbert, S. C. Smith and M. J. T. Jordan, *UNIMOL program suite* (*calculation of fall-off curves for unimolecular and recombination reactions*), Sydney University, 1993.
37 S. W. Benson, *Thermochemical Kinetics: Methods for Estimation of Thermochemical Data and Rate Parameters*, Wiley, New York, 1968.
38 R. Becerra, H. M. Frey, B. P. Mason, R. Walsh and M. S. Gordon, *J. Chem. Soc., Faraday Trans.*, 1995, **91**, 2723.
39 R. Becerra, S. E. Boganov, M. P. Egorov, O. M. Nefedov and R. Walsh, *Mendeleev Commun.*, 1997, **3**, 87.
40 N. Al-Rubaiey and R. Walsh, *J. Phys. Chem.*, 1994, **98**, 5303.
41 J. G. Gutsche, W. D. Lawrance, W. S. Staker and K. D. King, *J. Phys. Chem.*, 1995, **99**, 11867.
42 H. E. O'Neal, M. A. Ring, D. Kim and K. D. King, *J. Phys. Chem.*, 1995, **99**, 9397.
43 P. Devolder, C. Fittschen, A. Frenzel, H. Hippler, G. Poskrebyshev, F. Striebel and B. Viskolcz, *Phys. Chem. Chem. Phys.*, 1999, **1**, 675.
44 C. Fittschen, H. Hippler and B. Viskolcz, *Phys. Chem. Chem. Phys.*, 2000, **2**, 1677.